nature structural & molecular biology

Toll-like receptor 8 senses degradation products of single-stranded RNA

Hiromi Tanji[1,5], Umeharu Ohto[1,5], Takuma Shibata[2,3], Masato Taoka[4], Yoshio Yamauchi[4], Toshiaki Isobe[3,4], Kensuke Miyake[2] & Toshiyuki Shimizu[1,3]

Toll-like receptor 8 (TLR8) recognizes viral or bacterial single-stranded RNA (ssRNA) and activates innate immune systems. TLR8 is activated by uridine- and guanosine-rich ssRNA as well as by certain synthetic chemicals; however, the molecular basis for ssRNA recognition has remained unknown. In this study, to elucidate the recognition mechanism of ssRNA, we determined the crystal structures of human TLR8 in complex with ssRNA. TLR8 recognized two degradation products of ssRNA—uridine and a short oligonucleotide—at two distinct sites: uridine bound the site on the dimerization interface where small chemical ligands are recognized, whereas short oligonucleotides bound a newly identified site on the concave surface of the TLR8 horseshoe structure. Site-directed mutagenesis revealed that both binding sites were essential for activation of TLR8 by ssRNA. These results demonstrate that TLR8 is a sensor for both uridine and a short oligonucleotide derived from RNA.

Toll-like receptors (TLRs) are type I membrane glycoproteins that contain extracellular leucine-rich repeat (LRR), transmembrane and intracellular Toll–IL-1 receptor homology (TIR) domains[1,2]. TLRs recognize a wide range of ligands including lipopolysaccharide (recognized by the TLR4–MD-2 complex[3,4]), double-stranded RNA (recognized by TLR3 (ref. 5)) and lipoprotein (recognized by TLR2–TLR1 or TLR2–TLR6 heterodimers[6,7]). TLRs differ in their expression among different cell types. Their signal-transduction pathways also vary, being dependent on either myeloid differentiation primary response 88 (MyD88) or TIR domain–containing adaptor inducing interferon-β, on the basis of adaptor usage[8,9].

TLR7, TLR8 and TLR9 constitute a subfamily of proteins that recognize single-stranded nucleic acids[10]. TLR8 and TLR7 are closely related TLRs that can be activated by exogenous viral ssRNAs[11,12] such as those derived from influenza A virus[13], vesicular stomatitis virus[14], human immunodeficiency virus type 1 (ref. 12) and Coxsackie B virus[15] as well as by bacterial ssRNAs[16,17]. TLR8 and TLR7 can also be activated by endogenous RNAs, such as short interfering RNAs (siRNAs)[18–20] and self RNAs released from dead or dying cells, and can consequently contribute to autoimmune diseases such as systemic lupus erythematosus[21]. In particular, TLR7 and TLR8 recognize guanosine- and uridine-rich ssRNA[12,22,23]. These two receptors are also activated by certain chemical compounds[24–26]. Upon engagement of ssRNAs in endosomes, TLR7 and TLR8 initiate the Myd88-dependent pathway culminating in synthesis of interferons and proinflammatory mediators[24,27,28].

In a recent study, we demonstrated the structural basis for recognition of these small chemical ligands by TLR8 as well as the mechanism by which ligand binding activates the receptors[29]. However, it has remained unclear how TLR8 recognizes its natural ligand (ssRNA) and how the receptor can be activated by molecules as structurally and chemically different as ssRNA and the chemical ligands. To investigate these questions, we performed crystallographic studies of TLR8 in complex with ssRNAs. The resultant structures revealed that TLR8 recognizes, at distinct sites, uridine and a short oligonucleotide derived from degradation of ssRNA. These findings allow us to rationalize the activation mechanism of TLR8 by its natural ligand, and they could facilitate the development of drugs for treatment of viral infections and autoimmune diseases.

RESULTS

TLR8–ssRNA complex forms an activated dimer

We determined the crystal structures of the human TLR8 extracellular domain in complex with its 20-mer agonist ssRNAs[12,23]: ORN06, ssRNA40 and phosphorothioated ORN06 (ORN06S) (**Fig. 1**, **Table 1** and **Supplementary Figs. 1** and **2**). The ectodomain of the TLR8 protomer consisted of 26 LRRs with a Z loop (**Fig. 1b**,**c**). All structures of TLR8–ssRNA complexes (**Fig. 1d**,**e** and **Supplementary Fig. 1a**,**b**) were similar to the active forms of TLR8 dimers[29]: superposition of the three TLR8–ssRNA complexes and the TLR8–CL097 complex resulted in small r.m.s. deviations, 0.5–0.6 Å. Throughout this report, we indicate the second TLR8 in the dimer, as well as its individual residues, with asterisks.

Two binding sites for the degradation products of ssRNA

Unexpectedly, we did not observe electron density corresponding to the intact ORN06 20-mer in the TLR8–ORN06 structure. Instead, we

[1]Graduate School of Pharmaceutical Sciences, University of Tokyo, Tokyo, Japan. [2]Department of Microbiology and Immunology, Institute of Medical Science, University of Tokyo, Tokyo, Japan. [3]Core Research for Evolutional Science and Technology (CREST), Japan Science and Technology Agency (JST), Tokyo, Japan. [4]Department of Chemistry, Graduate School of Science and Technology, Tokyo Metropolitan University, Tokyo, Japan. [5]These authors contributed equally to this work. Correspondence should be addressed to T. Shimizu (shimizu@mol.f.u-tokyo.ac.jp).

Received 18 July 2014; accepted 1 December 2014; published online 19 January 2015; doi:10.1038/nsmb.2943

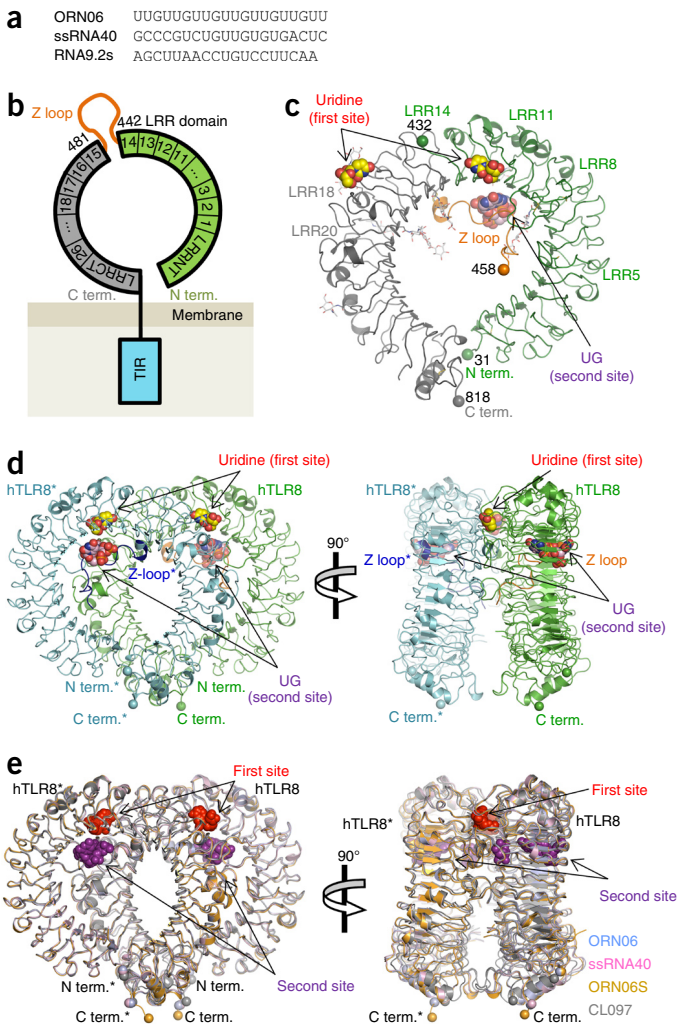

Figure 1 Structures of human TLR8. (**a**) ssRNA sequences used in this study. (**b**) Schematic representation of the domain organization of human (h) TLR8. The ring shape, the vertical line and the rectangular box show the extracellular LRR domain, the transmembrane domain and the intracellular TIR domain, respectively. LRRs are indicated by numbered boxes. The N-terminal half (N term.), the Z loop and the C-terminal half (C term.) are shown in green, orange and gray, respectively. (**c**) Front view of the protomer structure of the hTLR8–ORN06 dimer. The colors are the same as in **b**. Uridine in the first site and UG in the second site are shown in space-filling representations. N-glycans and disulfide bonds are shown as gray and yellow sticks, respectively. The N and C termini of each fragment are shown as spheres. The C, O, N and P atoms of the ligands are colored yellow (uridine) or purple (UG), red, blue and orange, respectively. (**d**) Front (left) and side (right) views of the TLR8–ORN06 dimer. TLR8 and its dimerization partner TLR8* are colored green and cyan, respectively. The Z loops are colored orange (TLR8) or blue (TLR8*). Uridine is recognized at the first site, within the dimerization interface, whereas UG is recognized at the second site, located on the concave face between the ring-shaped LRR structure and the Z loop. (**e**) Superposition of the overall structures. TLR8–RNA06, TLR8–ssRNA40, TLR8–RNA06S and TLR8–CL097 dimers are shown in cyan, magenta, orange and gray, respectively. Ligands at the first and second site are shown as red and purple spheres, respectively.

detected electron density corresponding to degradation products of the ssRNA at two distinct sites (first and second sites) (**Figs. 1c–e** and **2**). The first site was located at the same position where small chemical ligands bind[29], whereas the second site was located in the concave surface of TLR8 at a position not previously implicated in ligand binding. We unambiguously assigned the electron density at the first site as uridine, and the density at the second site was UG from the ORN06 sequence. To confirm that the observed mononucleoside and oligonucleotide were bona fide degradation products, rather than parts of intact ssRNA whose remaining structure was disordered or otherwise undetectable, we conducted LC-MS analyses of the dissolved TLR8–ORN06 crystals. Consistently with the structural analyses, we detected no intact ORN06 20-mer at all (**Fig. 3**) but did detect degradation products of ORN06. Uridine was the most abundant species, and two short oligonucleotides, UG and UUG, were also detectable. From our LC-MS analysis, we assumed that the electron density observed at the second site corresponded to a mixture of multiple species.

These results suggested that TLR8 bound products derived from degradation of ORN06 by unidentified nucleases and phosphatases, and that this interaction induced the active form of the TLR8 dimer. Consistently with these observations, we obtained a similar result with the TLR8–ssRNA40 complex (**Supplementary Figs. 1a** and **3a**,**b**). To avoid degradation, we incorporated ORN06S, which is more resistant to hydrolysis by RNases. Surprisingly, we still observed the degraded products, uridine and oligonucleotide, bound at the same sites (**Supplementary Figs. 1b** and **3c**,**d**).

Recognition of uridine mononucleoside at the first site

The first site consisted of LRR11–14 and LRR16*–18* (and LRR11*–14* and LRR16–18) (**Fig. 2a** and **Supplementary Fig. 4**). The uridine ribose moiety was surrounded by V378, K350, G351, Y348, V573* and T574*. The base moiety of the uridine was surrounded by R429, Y353, F405, V520* and D543*. Uridine formed several hydrogen bonds with TLR8: N3 with the D543* side chain, O4 with R429 and O2 indirectly with D543* and T574* N. All of the OH groups of the uridine ribose were involved in hydrogen bonds with TLR8: the 2′-OH group with the D545* side chain, the 3′-OH group with the G351* O and the 5′-OH group with the T574* N. The 3′-OH group also formed a water-mediated hydrogen bond with the I349 O and S352 O. The base moiety of uridine stacked onto the side chain of F405 similarly as observed in the complexes with chemical ligands (**Figs. 2a** and **4**). Notably, in addition to the interaction with uridine, R429 concurrently made hydrogen bonds with the A518* O, bridging TLR8, TLR8* and uridine.

In the TLR8–ssRNA40 structure, electron densities at the first site could be assignable to a pyrimidine mononucleoside. Although ssRNA40 had both uridine and cytidine in its sequence, we modeled uridine into the structure (**Supplementary Fig. 3a**) because uridine exhibited a higher affinity than cytidine, as described later. This mononucleoside was recognized in a similar manner to uridine in TLR8–ORN06 structure.

As compared to the recognition of chemical ligands, binding of uridine involved both conserved and unique structural features (**Fig. 4a–c**). Common features included stacking interactions between the aromatic rings of the ligands and F405 of TLR8. However, key interactions between the amidine groups of chemical ligands and D543* of TLR8 were partially collapsed in the TLR8–ORN06 complex. In the TLR8–chemical ligand complex, the alkyl substituent of the chemical ligand snugly fit into the hydrophobic pocket formed between the two protomers, whereas the hydrophobic pocket was unoccupied in the TLR8–ORN06 complex.

Recognition of oligonucleotide at the second site

The second site consisted of the concave surface of LRR10–13 and the ordered region of the Z loop (residues 469–474) (**Fig. 2a**

Table 1 Data collection and refinement statistics

	TLR8–ORN06	TLR8–ssRNA40	TLR8–ORN06S	TLR8–uridine
Data collection				
Space group	$P2_1$	$P2_1$	$P2_1$	$C222_1$
Cell dimensions				
a, *b*, *c* (Å)	86.7, 141.1, 169.5	86.3, 139.7, 167.6	86.7, 141.3, 170.0	105.4, 133.3, 120.0
β (°)	90.6	91.4	89.5	–
Resolution (Å)	2.0 (2.1–2.0)[a]	2.4 (2.53–2.40)	2.6 (2.64–2.60)	1.9 (1.93–1.90)
R_{merge}	0.107 (0.844)	0.098 (0.492)	0.148 (0.866)	0.067 (0.610)
$I / \sigma I$	9.8 (1.7)	8.8 (2.0)	22.2 (1.9)	19.2 (1.7)
Completeness (%)	97.6 (96.6)	93.0 (87.2)	99.8 (100.0)	98.9 (99.8)
Redundancy	4.4 (4.3)	3.4 (3.0)	3.8 (3.7)	3.6 (3.3)
Refinement				
Resolution (Å)	33.7–2.0	41.2–2.4	31.6–2.6	48.6–1.9
No. reflections	253,971	136,666	115,689	61,985
R_{work} / R_{free}	0.190 / 0.234	0.194 / 0.257	0.220 / 0.285	0.203 / 0.260
No. atoms				
Protein	23,834	23,803	24,106	5,995
First site	68	68	68	17
Second site	188	188	192	–
Water	1,434	925	–	330
B factors				
Protein	42.2	48.0	64.2	37.2
First site	27.0	29.0	46.7	27.6
Second site	50.9	45.8	62.9	–
Water	40.6	34.9	–	35.4
r.m.s. deviations				
Bond lengths (Å)	0.011	0.009	0.011	0.013
Bond angles (°)	1.63	1.48	1.32	1.65

Each data set was collected with one crystal.
[a]Values in parentheses are for highest-resolution shell.

and **Supplementary Fig. 4**). The UG at the second site of the TLR8–ORN06 structure was located outside the dimerization interface, thus indicating that the second site does not directly contribute to dimerization (**Supplementary Fig. 1c**).

We observed several characteristic interactions between UG and TLR8 (**Fig. 2a**). The phosphate group of guanosine interacted with the H469 side chain. The guanosine ring was sandwiched between the side chains of H373 (LRR12) and H469 (Z loop), and it made four hydrogen bonds with TLR8: N1 and N2 with D343, and O6 and N7 with R375. In the TLR8–ssRNA40 structure, we also observed similar electron density corresponding to a pyrimidine-purine dinucleotide at the second site and assigned it tentatively as UG (**Fig. 4b** and **Supplementary Fig. 3b**), although the identity of the bases could not be determined because multiple alternatives, UG and CG, could have accounted for the observed density (**Fig. 1a** and **Supplementary Fig. 2b**). In the TLR8–ORN06S structure, we observed UG at the second site (**Supplementary Figs. 2c** and **3d**). The UG in TLR8–ORN06, TLR8–ssRNA40 and TLR8–ORN06S adopted different conformations: only the guanosine moiety, sandwiched between two histidines, occupied the same position in both structures (**Supplementary Fig. 1d**). Hence, the second site seemed to prefer short oligonucleotides containing guanosine, but the mode of recognition was not strict.

Functional importance of the first and second sites

To confirm the functional importance of the first and second sites of TLR8 in ssRNA recognition, we mutated the first- and second-site residues to alanine and examined the ability of the resultant mutants to activate nuclear factor κB (NF-κB) in a reporter gene assay (**Fig. 2b**). The first-site mutation F405A abolished responses to both ssRNA and chemical ligands. Likewise, D543A, Y348A and T574A mutations completely abolished or substantially weakened the ability to activate NF-κB, as we have previously reported[29]. However, the second-site mutations H373A, R375A, Y468A, F470A and L474A, all of which modified residues that made contact with the UG dinucleotide, specifically diminished activation in response to ssRNA but did not alter the response to chemical ligands. These results suggested that both sites are essential for ssRNA recognition by TLR8, whereas the second site is not essential for recognition of chemical ligands. In the TLR8–ssRNA complex, the R429 side chain adopted a conformation distinct from that in complexes containing chemical ligands and formed hydrogen bonds with the uridine O4 atom (**Figs. 2a** and **4**, and **Supplementary Fig. 3a**,**c**). We did not observe this interaction in complexes containing chemical ligands. Accordingly, the mutation of R429 abolished the responsiveness of TLR8 to ssRNA (**Fig. 2b**) but not to chemical ligands[29].

TLR8 is a uridine sensor

From the structural analyses, we hypothesized that, among mononucleosides, TLR8 exhibited a preference for uridine. To test this idea, we conducted isothermal titration calorimetry (ITC) analysis to determine the affinity of TLR8 for each mononucleoside in solution as well as for the chemical ligand R848. As predicted, among the mononucleosides, uridine exhibited the highest affinity for TLR8, with a K_d of 55 μM (**Fig. 5a**). For mononucleosides other than uridine, the heat released or absorbed upon TLR8-ligand interaction was too small to determine the affinity constants. The first site could not accommodate a mononucleotide or oligonucleotide because both the 5′- and 3′-OH groups of the uridine ribose moiety were involved in hydrogen bonds with TLR8 and were thus partially buried in the dimerization interface (**Figs. 2a** and **4**). In fact, neither 5′-UMP nor 3′-UMP released or absorbed heat in the ITC experiment (**Fig. 5a**).

Our present work suggests that oligonucleotide binding to the second site influences uridine binding to the first site. Therefore, we performed NF-κB–dependent luciferase reporter assays, using HEK293T cells stimulated with uridine and oligonucleotide (ORN06S). Expectedly, we clearly observed the synergistic immunostimulatory effect for uridine and oligonucleotide but not for other nucleosides (adenosine, guanosine, cytidine, thymidine and inosine) and oligonucleotide (**Fig. 5b**). We performed the experiment with suboptimal concentrations of ORN06S to allow the observation of synergistic effects. In this condition, uridine or oligonucleotide alone did not exhibit activity. Furthermore, we quantitatively assessed the synergistic effect by ITC. The resultant K_d value for uridine in the presence of oligonucleotide greatly increased, to 1.0 μM (**Fig. 5b**), a value comparable to that of the synthetic ligand. The length of the oligonucleotide for the second site was not limiting because the second site was located outside the dimerization interface, accommodating

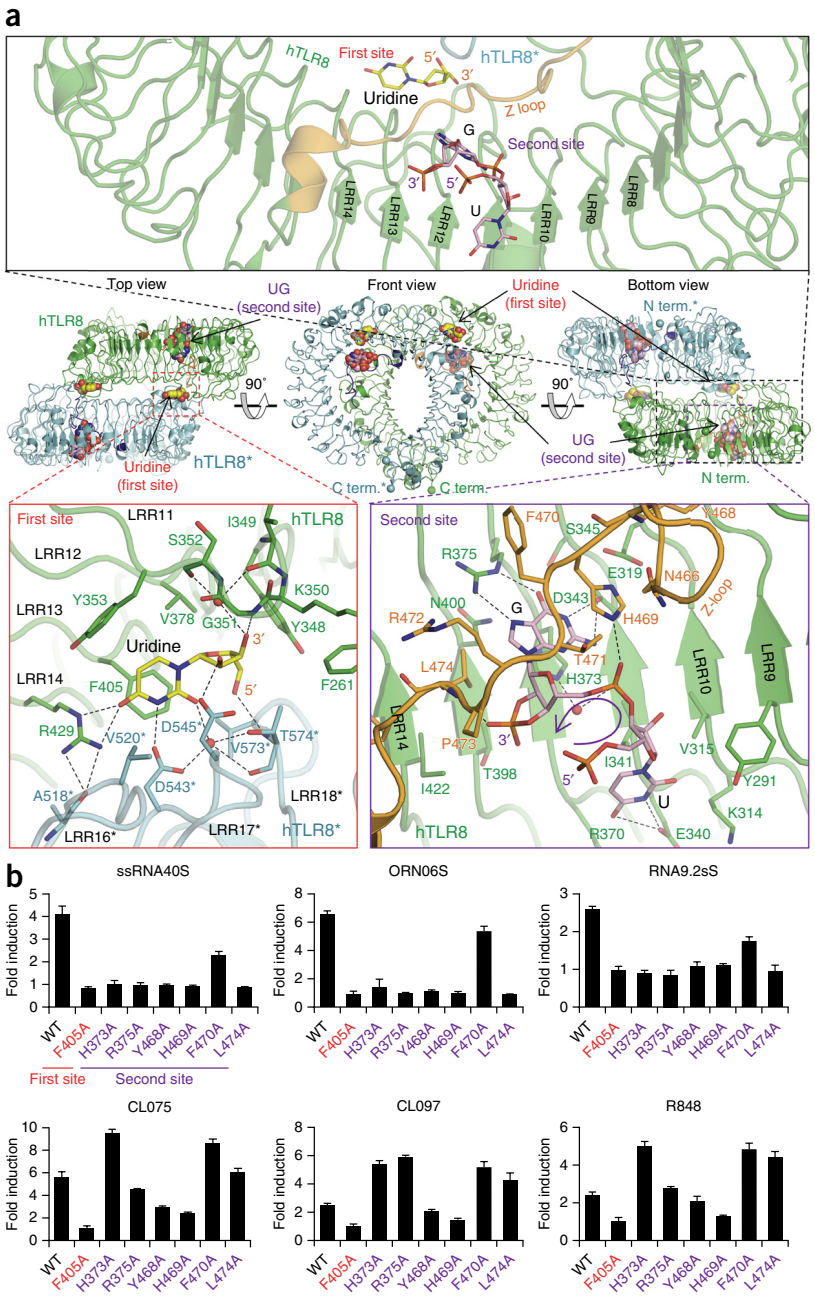

Figure 2 ssRNA recognition by TLR8. (**a**) Detailed views of human TLR8 in complex with ORN06. Top, magnified views of the first and second sites of TLR8–ORN06. Middle, top, front and bottom views of the TLR8–ORN06 dimer. Bottom, magnified views of the first (left) and second (right) sites. Uridine at the first site and UG at the second site are shown in yellow and purple, respectively. Water molecules mediating ligand recognition are indicated by red spheres. Hydrogen bonds are indicated by dashed lines. (**b**) NF-κB activity of human TLR8 mutants in HEK293T cells, stimulated by ssRNA40S, ORN06S and RNA9.2sS[18] (ssRNAs with S suffix indicating phosphorothioation), and CL075, CL097 and R848 (small chemical ligands). Error bars, s.d. ($n = 3$ independent experiments). WT, wild type.

the longer oligonucleotide as well as a dinucleotide. In fact, intact ORN06 bound to TLR8 with a K_d value of 4.8 μM (**Fig. 5**).

We also crystallized TLR8 in complex with uridine (**Table 1** and **Supplementary Figs. 2d** and **5**). The resultant TLR8–uridine crystal structure contained an active form of the TLR8 dimer, with an r.m.s. deviation of 1.1 Å relative to the structure of TLR8–ORN06. We observed clear electron density corresponding to uridine at the first site (**Supplementary Fig. 2d**). Uridine in TLR8–uridine and TLR8–ORN06 was recognized virtually identically.

DISCUSSION

Several groups have investigated the sequence specificity of the ssRNAs that activate TLR8 (refs. 12,22,23), and our previous crystallographic study revealed the mechanism of activation of TLR8 by small chemical ligands[29]. Regardless, the mechanism by which ssRNA activates TLR8 has remained largely unknown, in part because ssRNA is structurally and chemically so different from small chemical ligands.

Our structural studies, combined with biochemical and biophysical analyses, help to elucidate this mechanism. The structures reveal that TLR8 binds degradation products of ssRNA at two distinct sites. The first site prefers uridine mononucleoside (**Fig. 5**). Nonetheless, the affinity of uridine for TLR8 ($K_d = 55$ μM) is still lower than the affinities of chemical ligands ($K_d = 0.20$ μM). However, the K_d value of uridine for TLR8 in the presence of oligonucleotide was greatly increased, to 1.0 μM, thus implying that uridine alone cannot activate TLR8 efficiently under physiological conditions, but the presence of the second binding site compensates for the relatively low affinity of uridine. Chemical ligands exhibit sufficiently high affinity to activate TLR8 by themselves, whereas the synergistic cooperation of uridine and oligonucleotide makes it possible to exhibit an immunostimulatory effect.

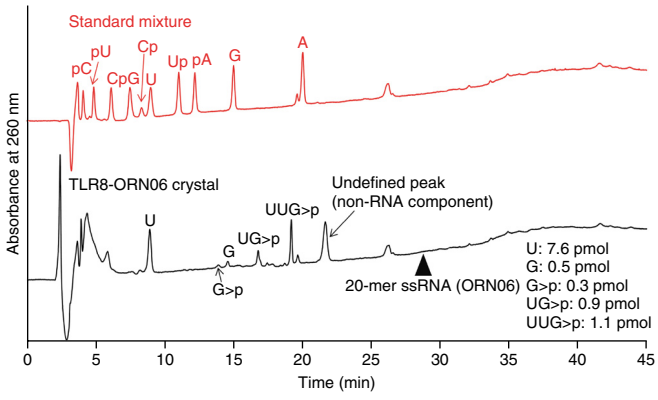

Figure 3 LC-MS analyses of dissolved TLR8–ORN06 crystals. The LC elution profiles of standard nucleosides and nucleotides (red) and RNA components of the TLR8–ORN06 crystal (black) are shown. The figure also indicates an approximate amount of each RNA component found in the crystal sample (~10 pmol). The arrowhead shows the elution position of the 20-mer ssRNA ORN06. pU, Up and G>p denote uridine 5′-monophosphate, uridine 3′-monophosphate and guanine 2′,3′-cyclic monophosphate, respectively.

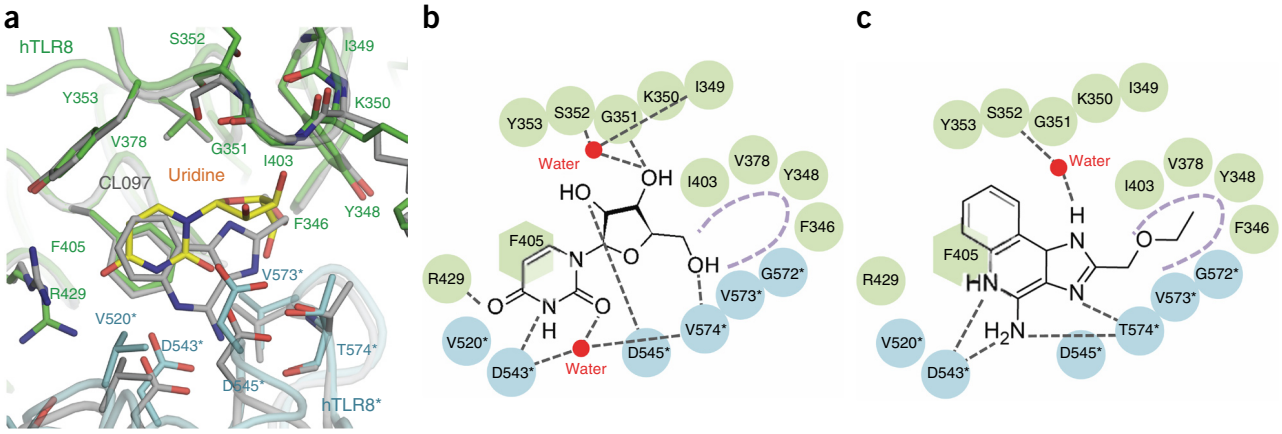

Figure 4 Ligand recognition at the first site of TLR8. (**a**) Superposition of TLR8–ORN06 and TLR8–CL097 (chemical ligand). Uridine in TLR8–ORN06 is shown in yellow; CL097 in TLR8–CL097 is shown in gray. (**b**) Schematic representation of interactions between TLR8 and uridine. Hydrogen bonds are shown as dashed lines. The hydrophobic pocket, shown as arcs, is unoccupied. (**c**) Schematic representation of interactions between TLR8 and the chemical ligand CL097.

The oligonucleotide binding to the second site itself would not induce the activated form of the TLR8 dimer because the second site is located outside the dimerization interface (**Fig. 2a** and **Supplementary Fig. 1c**). We hypothesize that although uridine binding to the first site directly induces the activated form of the TLR8 dimer, oligonucleotide binding to the second site allosterically promotes uridine binding to the first site, possibly by stabilizing the Z loop and surrounding residues in favor of the activated form (**Fig. 6**), thus exhibiting a synergistic immunostimulatory effect. In fact, small-angle X-ray scattering (SAXS) analysis showed that the scattering curves for ligand-free TLR8 and TLR8 complexed with ORN06 were very similar, whereas the curve for the TLR8–R848 complex exhibited a distinct pattern (**Supplementary Fig. 6**), thus indicating that RNA binding would not induce the activated form.

Our present work suggests that RNAs having enough uridines would have immunostimulatory potential. Initially, ssRNA40 from the U5 region of HIV-1 was previously identified as a natural agonist of TLR7 and TLR8, and GU-rich ssRNA was proposed to be a natural ligand for TLR7 and TLR8 (ref. 12). Forshbach *et al.* proposed that AU-rich RNAs mediate human TLR8 activation and that GU-rich RNAs stimulate human TLR7 and TLR8 immune responses[23]. Accordingly, ssRNA40 activates TLR8, whereas ssRNA41

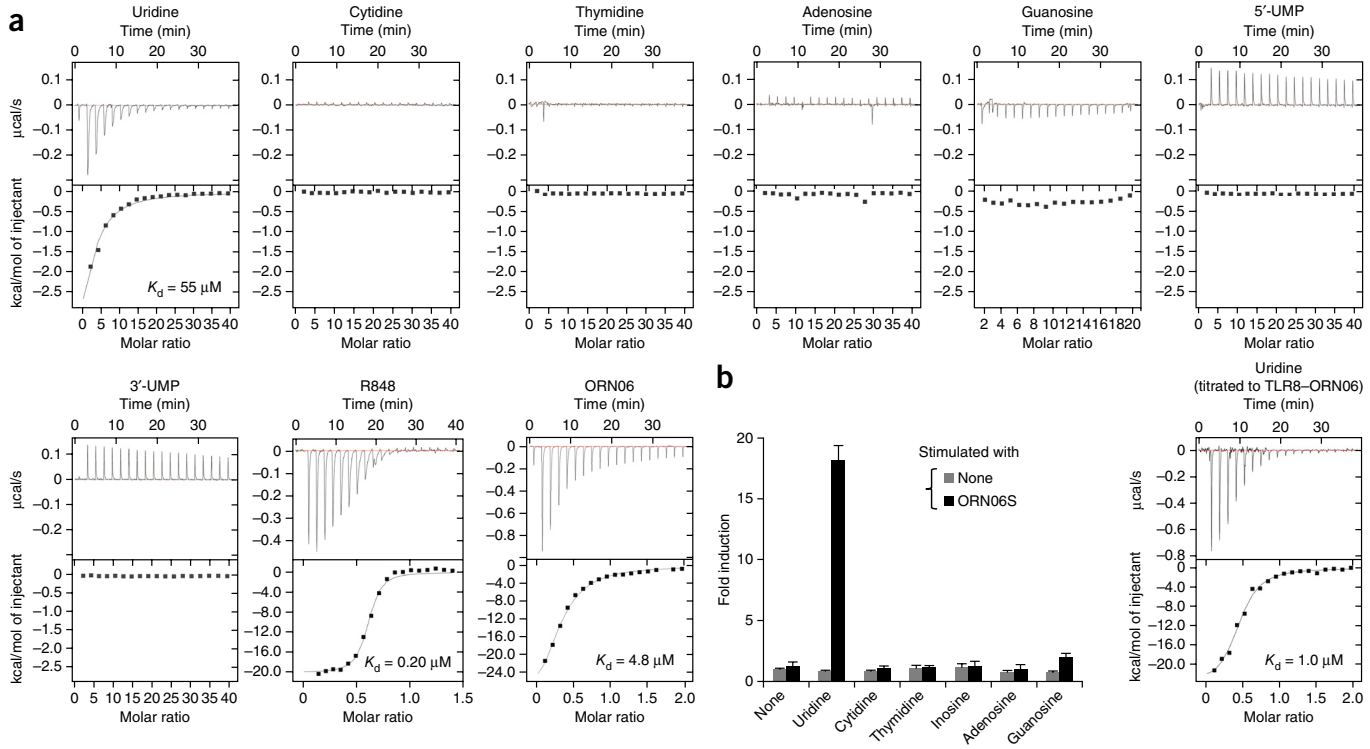

Figure 5 Binding affinities for mononucleosides and a synergistic effect of uridine and oligonucleotide. (**a**) ITC analysis of hTLR8 with mononucleosides (uridine, cytidine, thymidine, guanosine and adenosine), uracil-containing mononucleotides (5′-UMP and 3′-UMP), the chemical ligand R848 and ORN06. (**b**) Left, NF-κB activity of human TLR8 mutants in HEK293T cells, stimulated by nucleosides with or without 2.5 µg/ml ORN06S. Error bars, s.d. (n = 3 independent experiments). Right, ITC analyses of hTLR8 with uridine in the presence of ORN06.

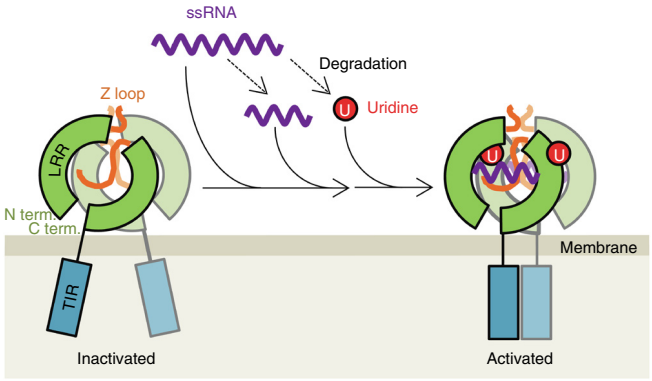

Figure 6 Proposed mechanism of TLR8 activation by binding of ssRNA. The ligand-free, inactivated form of TLR8 (left) transforms into the activated form (right) upon binding of degradation products derived from ssRNA. The first site, in the same position as the previously identified binding site for chemical ligands, prefers uridine.

(GCCCGACAGAAGAGAGACAC), a derivative of ssRNA40 in which uridines are replaced with adenosines, cannot activate TLR8 at all. However, TLR8 has been shown to strongly induce NF-κB activation upon stimulation with ssRNA42 (G-to-A–substituted ssRNA40)[12], and poly(U) has been shown to exhibit an immunostimulatory effect[11], thus suggesting that GU is not necessarily required. Li *et al.* reported that ssRNA120 (GUCUGAGUGUGUUCUUG) induced TNF-α release, whereas U-to-A–substituted fakeRNA120 (GACAGAGAGAGAACAAG) lost its stimulatory activity toward TLR8 (ref. 30). A substantial number of immunostimulatory single-stranded siRNAs contain a high level of uridines, and replacement of uridines with adenosines has been shown to reduce immune activation[20]; in contrast, the stimulatory RNA has been shown to contain GU-rich sequence[31]. It was also reported that single-stranded siRNAs with very low GU content or without a GU sequence also activate the immune system[20]. Hence, some sequence specificity of RNA agonists for TLR8 and TLR7 has been observed, but the sequence specificity is not well established because it seems to be 'loose'. These studies have demonstrated that uridine is the most critical nucleoside for TLR8 activation. However, several microRNAs (miRNAs) have been shown to activate TLR8, and one miRNA containing uridines was reported to be unable to induce cytokine secretion[32]. Although it is difficult to comprehensively explain all the results for TLR8 activation by ssRNA, our findings demonstrate that TLR8-agonist RNAs exhibit loose RNA sequence specificity.

Additional studies have shown that viral genomic ssRNA exhibits an immunostimulatory effect[11]. Moreover, *in vitro*–transcribed long RNAs (on the order of kilobases) as well as bacterial total RNA were able to stimulate HEK293 cells stably expressing human TLR8, and mitochondrial RNA isolated from human platelets also stimulated human TLR8 (ref. 33). In contrast, long RNA such as mammalian tRNA did not induce any detectable level of TNF-α (ref. 33). Some uridine-containing RNAs exhibited no immunogenicity, probably owing to nucleoside modifications, formation of nuclease-resistant secondary structures or transport of the RNA to lysosomes.

According to our structural work, double-stranded RNA (dsRNA) itself is unlikely to bind to TLR8 directly; thereby, dsRNA would be unable to function as a TLR8 agonist. Our present work suggests that RNA should be partly degraded to produce uridine and oligonucleotide for the immunostimulatory effect. RNA is likely to be degraded in lysosomes because lysosomes contain many different hydrolytic enzymes, including nucleases and phosphatases, but a degradation process under physiological conditions remains unidentified. Because dsRNA is more resistant to nuclease[18], ssRNA should exhibit a stronger effect. In fact, the single-stranded siRNAs were highly immunostimulatory compared to their double-stranded siRNA counterparts[19].

This study does not comprehensively address the length and sequence determinants of oligonucleotide binding to the second site of TLR8. However, our findings make it clear that guanosine-containing sequence is preferable, whereas the length of the oligonucleotide is immaterial: the LC-MS analysis revealed that crystals of TLR8–ORN06 contained both 2-mer (UG) and 3-mer (UUG) oligonucleotides (**Fig. 3**). TLR8 can be activated by the ssRNA ORN02 ($(UUA)_6UU$), which contains only uridine and adenosine[23]; therefore, it is likely that guanosine can be replaced by adenosine. Hence, we presume that any oligonucleotide longer than a 2-mer and containing a purine base would bind the second site.

Our structure of TLR8 in complex with ssRNA redefines the role of TLR8 as a uridine sensor in the presence of oligonucleotide. The new finding that TLR8 has two ligand-binding sites advances understanding of the RNA-recognition mechanism of TLR8, and it should also facilitate the development of therapeutic drugs targeting this receptor.

METHODS

Methods and any associated references are available in the online version of the paper.

Accession codes. Coordinates and structure factors for human TLR8–ORN06 (PDB 4R07), TLR8–ssRNA40 (PDB 4R08), TLR8–ORN06S (PDB 4R09) and TLR8–uridine (PDB 4R0A) complexes have been deposited in the Protein Data Bank.

Note: Any Supplementary Information and Source Data files are available in the online version of the paper.

ACKNOWLEDGMENTS

We thank the beamline staff members at Photon Factory and SPring-8 for their assistance with data collection. We also thank M. Osawa and I. Shimada for their help with the ITC data acquisition. This work was supported by Grants-in-Aid from the Japan Society for the Promotion of Science KAKENHI, grant nos. 25121709, 25115504, 26711002 (U.O.), 25860354 (T. Shibata), 25253032 (K.M.), 23116007 and 25291010 (T. Shimizu); by the Takeda Science Foundation (U.O. and T. Shimizu); and by the Mochida Memorial Foundation for Medical and Pharmaceutical Research (U.O.).

AUTHOR CONTRIBUTIONS

H.T. and U.O. performed the crystallization and structure determination. T. Shibata and K.M. performed the functional analyses. M.T., Y.Y. and T.I. performed LC-MS. H.T., U.O., T. Shibata, K.M. and T. Shimizu analyzed the results. All authors contributed to writing the manuscript.

COMPETING FINANCIAL INTERESTS

The authors declare no competing financial interests.

1. Song, D.H. & Lee, J.O. Sensing of microbial molecular patterns by Toll-like receptors. *Immunol. Rev.* **250**, 216–229 (2012).
2. Akira, S. & Takeda, K. Toll-like receptor signalling. *Nat. Rev. Immunol.* **4**, 499–511 (2004).
3. Poltorak, A. *et al.* Defective LPS signaling in C3H/HeJ and C57BL/10ScCr mice: mutations in *Tlr4* gene. *Science* **282**, 2085–2088 (1998).
4. Shimazu, R. *et al.* MD-2, a molecule that confers lipopolysaccharide responsiveness on Toll-like receptor 4. *J. Exp. Med.* **189**, 1777–1782 (1999).
5. Alexopoulou, L., Holt, A.C., Medzhitov, R. & Flavell, R.A. Recognition of double-stranded RNA and activation of NF-κB by Toll-like receptor 3. *Nature* **413**, 732–738 (2001).

6. Alexopoulou, L. *et al.* Hyporesponsiveness to vaccination with *Borrelia burgdorferi* OspA in humans and in TLR1- and TLR2-deficient mice. *Nat. Med.* **8**, 878–884 (2002).
7. Takeuchi, O. *et al.* Cutting edge: role of Toll-like receptor 1 in mediating immune response to microbial lipoproteins. *J. Immunol.* **169**, 10–14 (2002).
8. Akira, S. TLR signaling. *Curr. Top. Microbiol. Immunol.* **311**, 1–16 (2006).
9. Kawai, T. & Akira, S. The role of pattern-recognition receptors in innate immunity: update on Toll-like receptors. *Nat. Immunol.* **11**, 373–384 (2010).
10. Roach, J.C. *et al.* The evolution of vertebrate Toll-like receptors. *Proc. Natl. Acad. Sci. USA* **102**, 9577–9582 (2005).
11. Diebold, S.S., Kaisho, T., Hemmi, H., Akira, S. & Sousa, C.R.E. Innate antiviral responses by means of TLR7-mediated recognition of single-stranded RNA. *Science* **303**, 1529–1531 (2004).
12. Heil, F. *et al.* Species-specific recognition of single-stranded RNA via toll-like receptor 7 and 8. *Science* **303**, 1526–1529 (2004).
13. Wang, J.P. *et al.* Toll-like receptor-mediated activation of neutrophils by influenza A virus. *Blood* **112**, 2028–2034 (2008).
14. Lund, J.M. *et al.* Recognition of single-stranded RNA viruses by Toll-like receptor 7. *Proc. Natl. Acad. Sci. USA* **101**, 5598–5603 (2004).
15. Triantafilou, K. *et al.* Human cardiac inflammatory responses triggered by Coxsackie B viruses are mainly Toll-like receptor (TLR) 8-dependent. *Cell. Microbiol.* **7**, 1117–1126 (2005).
16. Cervantes, J.L. *et al.* Human TLR8 is activated upon recognition of *Borrelia burgdorferi* RNA in the phagosome of human monocytes. *J. Leukoc. Biol.* **94**, 1231–1241 (2013).
17. Gantier, M.P. *et al.* Genetic modulation of TLR8 response following bacterial phagocytosis. *Hum. Mutat.* **31**, 1069–1079 (2010).
18. Hornung, V. *et al.* Sequence-specific potent induction of IFN-α by short interfering RNA in plasmacytoid dendritic cells through TLR7. *Nat. Med.* **11**, 263–270 (2005).
19. Sioud, M. Induction of inflammatory cytokines and interferon responses by double-stranded and single-stranded siRNAs is sequence-dependent and requires endosomal localization. *J. Mol. Biol.* **348**, 1079–1090 (2005).
20. Sioud, M. Single-stranded small interfering RNA are more immunostimulatory than their double-stranded counterparts: a central role for 2′-hydroxyl uridines in immune responses. *Eur. J. Immunol.* **36**, 1222–1230 (2006).
21. Barrat, F.J. *et al.* Nucleic acids of mammalian origin can act as endogenous ligands for Toll-like receptors and may promote systemic lupus erythematosus. *J. Exp. Med.* **202**, 1131–1139 (2005).
22. Diebold, S.S. *et al.* Nucleic acid agonists for Toll-like receptor 7 are defined by the presence of uridine ribonucleotides. *Eur. J. Immunol.* **36**, 3256–3267 (2006).
23. Forsbach, A. *et al.* Identification of RNA sequence motifs stimulating sequence-specific TLR8-dependent immune responses. *J. Immunol.* **180**, 3729–3738 (2008).
24. Hemmi, H. *et al.* Small anti-viral compounds activate immune cells via the TLR7 MyD88-dependent signaling pathway. *Nat. Immunol.* **3**, 196–200 (2002).
25. Jurk, M. *et al.* Human TLR7 or TLR8 independently confer responsiveness to the antiviral compound R-848. *Nat. Immunol.* **3**, 499 (2002).
26. Kokatla, H.P. *et al.* Structure-based design of novel human Toll-like receptor 8 agonists. *ChemMedChem* **9**, 719–723 (2014).
27. Honda, K. *et al.* IRF-7 is the master regulator of type-I interferon-dependent immune responses. *Nature* **434**, 772–777 (2005).
28. Kawai, T. *et al.* Interferon-α induction through Toll-like receptors involves a direct interaction of IRF7 with MyD88 and TRAF6. *Nat. Immunol.* **5**, 1061–1068 (2004).
29. Tanji, H., Ohto, U., Shibata, T., Miyake, K. & Shimizu, T. Structural reorganization of the Toll-like receptor 8 dimer induced by agonistic ligands. *Science* **339**, 1426–1429 (2013).
30. Li, Y. *et al.* Extraordinary GU-rich single-strand RNA identified from SARS coronavirus contributes an excessive innate immune response. *Microbes Infect.* **15**, 88–95 (2013).
31. Vollmer, J. *et al.* Immune stimulation mediated by autoantigen binding sites within small nuclear RNAs involves Toll-like receptors 7 and 8. *J. Exp. Med.* **202**, 1575–1585 (2005).
32. Fabbri, M. *et al.* MicroRNAs bind to Toll-like receptors to induce prometastatic inflammatory response. *Proc. Natl. Acad. Sci. USA* **109**, E2110–E2116 (2012).
33. Karikó, K., Buckstein, M., Ni, H. & Weissman, D. Suppression of RNA recognition by Toll-like receptors: the impact of nucleoside modification and the evolutionary origin of RNA. *Immunity* **23**, 165–175 (2005).

ONLINE METHODS

Protein expression, purification and crystallization. The DNA encoding the extracellular domain of human Toll-like receptor 8 (hTLR8, residues 27–827), which was fused to a C-terminal thrombin-cleavage site located upstream of a protein A tag, was inserted into the expression vector pMT-BiP-V5-His of the *Drosophila* Expression System (Life Technologies). *Drosophila* S2 cells were cotransfected with the hTLR8 and pCoHygro vectors. Stably transfected cells were selected in Sf-900 II SFM medium containing 300 μg/mL hygromycin. Protein expression was induced by addition of 0.5 mM $CuSO_4$ in EXPRESS FIVE SFM medium. The culture medium was supplemented with kifunensine (1.5 mg/L) to produce protein with endoglycosidase-susceptible N-glycans. Culture supernatant was harvested at 160 h after induction. hTLR8 protein was purified by IgG Sepharose affinity chromatography, protein A–tag cleavage by thrombin, saccharide trimming by endo Hf and Superdex 200 gel-filtration chromatography followed by HiTrap Q anion-exchange chromatography. Purified hTLR8 was concentrated to 10–14 mg/mL in 50 mM MES, pH 5.5, and 50 mM NaCl.

The protein solutions for hTLR8–ssRNAs contained hTLR8 (7–8 mg/mL) and each ssRNA (protein/ssRNA molar ratio of 1:1) in a crystallization buffer containing 40 mM MES, pH 5.5, and 40 mM NaCl. The protein solution for hTLR8–uridine contained hTLR8 (8 mg/mL) and uridine (protein/uridine molar ratio of 1:10) in a crystallization buffer containing 40 mM MES, pH 5.5, and 40 mM NaCl. Crystallization experiments were performed with sitting-drop vapor-diffusion methods at 293 K. Crystals of TLR8–ssRNAs and TLR8–uridine complexes were obtained with reservoir solutions containing 12–14% (w/v) PEG 3350, 0.2–0.3 M potassium formate and 0.1 M sodium citrate, pH 4.8–5.2.

Data collection and structure determination. Diffraction data sets were collected with a wavelength of 1.0000 Å on beamlines PF-5A, PF-AR NE3A (Ibaraki, Japan) and SPring-8 BL41XU (Hyogo, Japan) under cryogenic conditions at 100 K. Crystals were soaked into a cryoprotectant solution containing 40 mM MES, pH 5.5, 40 mM NaCl, 0.15 M sodium formate, 75 mM sodium citrate, pH 4.8–5.2, 12–14% (w/v) PEG 3350 and 15–25% glycerol and were flash cooled in the cryostream. The data sets were processed with the HKL2000 package[34] or imosflm[35]. The structures of hTLR8–ssRNAs and hTLR8–uridine were determined by the molecular-replacement method with Molrep[36] with the hTLR8–CL097 structure (PDB 3W3J)[29]. The models were refined with stepwise cycles of manual model building with COOT[37] and were subjected to restrained refinement with REFMAC[38] or phenix.refine[39] until the *R* factors were converged. Ligand molecules, N-glycans and water molecules were modeled into the electron density maps at the latter cycles of the refinement. The quality of the final structure was evaluated with PROCHECK[40]. In structures of hTLR8–ORN06, hTLR8–ssRNA40, hTLR8–ORN06S and hTLR8–uridine, 100%, 99%, 100% and 99% of the residues were in Ramachandran favored or allowed regions, respectively. The statistics of the data collection and refinement are summarized in **Table 1**. The figures representing structures were prepared with PyMOL (http://www.pymol.org/).

Small-angle X-ray scattering. SAXS data were collected on SPring-8 BL45XU (Hyogo, Japan) at 293 K with a PILATUS 300K-W detector (DECTRIS) with a sample-to-detector distance of 2.0 m. The wavelength of the X-rays was set to 1.0000 Å. The solution of ligand-free hTLR8 contained 3 mg/ml hTLR8 in 50 mM MES, pH 5.5, and 0.2 M NaCl. The solution of the hTLR8–R848 complex contained 3 mg/ml hTLR8 and R848 (hTLR8/R848 molar ratio of 1:10) in 50 mM MES, pH 5.5, and 0.2 M NaCl. The solution of the hTLR8–ORN06 complex contained 1 mg/ml hTLR8 and ORN06 (hTLR8/ORN06 molar ratio of 1:1) in 8 mM MES, pH 5.5, and 0.1 M NaCl. $I(q)$ was obtained from SAXS experiments, where $q = 4\pi\sin\theta/\lambda$ (with 2θ as the scattering angle and λ as the X-ray wavelength).

Isothermal titration calorimetry. ITC experiments were done in a buffer composed of 10 mM MES, pH 5.5, and 100 mM NaCl at 298 K with a MicroCal iTC_{200} (GE Healthcare). The titration sequence included a single 0.4-μl injection followed by 18 injections of 2 μl each, with a spacing of 120 s between the injections. The titration conditions were as follows: 200 μM R848 into 30 μM hTLR8; 2 mM mononucleoside (uridine, cytidine, thymidine and adenosine) or uracil-containing mononucleotide (5′-UMP and 3′-UMP) into 10 μM hTLR8; 1 mM guanosine into 10 μM hTLR8; 0.2 mM uridine into 20 μM hTLR8 and 40 μM ORN06; or 0.3 mM ORN06 into 30 μM hTLR8. OriginLab software (GE Healthcare) was used to analyze the raw ITC data. Thermodynamic parameters were extracted from curve-fitting analysis with a single-site binding model. hTLR8–uridine data were analyzed with a fixed N value of 0.80.

Liquid chromatography–mass spectrometry analysis of RNA. An hTLR8–ORN06 crystal sample (~10 pmol) was washed five times with 30% 2-methyl-2, 4-pentanediol in 10 mM sodium citrate buffer, pH 4.6, dissolved into 5 μL of 10 mM MES, pH 5.5, containing 50 mM NaCl, and was applied to a reversed-phase LC-MS analysis of RNAs. The reversed-phase LC was performed on a column (2 mm i.d. × 100 mm) of Develosil C30-UG-3 (particle size 3 μm; Nomura Chemical) with a 30-min linear gradient from 2% to 18% acetonitrile in 10 mM triethylammonium acetate, pH 7.0, containing 10 μM ammonium phosphate at a flow rate of 100 μL/min. The eluate was monitored at 260 nm with a UV detector equipped with a semimicro flow cell (2.5-μL volume, 5-mm light path; SPD-20A, Shimadzu) and then analyzed by MS with a quadrupole-Orbitrap hybrid mass spectrometer (Q Exactive, Thermo Fisher Scientific, Inc.) connected in tandem with the UV detector through an electrospray ionization interface. Standard mixture (5 pmol each) was applied. The mass spectrometer was operated in a negative mode, switching automatically between MS and MS/MS acquisition as described[41].

NF-κB–dependent luciferase reporter assay. We previously described the luciferase reporter assay to detect NF-κB activation by hTLR8 (ref. 29). In brief, 5×10^5 HEK293T cells seeded in collagen-coated six-well plates were transiently transfected with wild-type or mutant hTLR8 cDNAs in pMX-puro-IRES-rat CD2 (1 μg), together with pELAM1-luc reporter plasmid (5 ng), with polyethylenimine 'Max' (Polysciences). HEK293T cells were cultured in DMEM (Gibco) with 10% FBS, 2 mM L-glutamine (Gibco) and 50 μM 2-ME. 36 h after transfection, transfected cells, reseeded in collagen-coated flat 96-well plates (Corning) at a density of 1×10^5 cells per well, were stimulated with 25 μg/ml ssRNAs or 5 μg/ml small chemical ligands for 6 h and subjected to luciferase assay with the Luciferase Assay System from Promega (**Fig. 2b**). To check nucleoside response in the presence of ssRNA (**Fig. 5b**), HEK293T cells with pELAM1-luc and human TLR8 were stimulated for 6 h with 1 mM nucleosides and 2.5 μg/ml ORN06S complexed with 30 μl/ml *N*-[1-(2,3-dioleoyloxy)propyl]-*N*,*N*,*N*-trimethylammonium methyl sulfate (DOTAP). In the absence of nucleoside, ssRNA alone at this concentration did not exhibit activity. CL075, CL097 and R848 were commercially prepared (Invivogen). ssRNA40S (GsCsCsCsGsUsCsUsGsUsUsGsUsGsUsGsAsCsUsC), ORN06S (UsUsGsUsUsGsUsUsGsUsUsGsUsUsGsUsUsGsUsU) and RNA9.2sS (UsGsUsCsCsUsUsCsAsAsUsGsUsCsCsUsUsCsAsA), in which 'S' denotes a phosphothioate linkage, were synthesized by FASMAC (Kanagawa, Japan). The relative light units of chemiluminescence were measured with a GloMax 96 Microplate Luminometer (Promega). Transfection efficiency of wild-type and mutant hTLR8 was checked by cell-surface expression of rat CD2 on HEK293T cells with a FACSCalibur flow cytometer. PE anti-rat CD2 (clone OX-34) was purchased from BioLegend (validation information on manufacturer's website) and used at the concentration of 200 ng/ml.

34. Otwinowski, Z. & Minor, W. Processing of X-ray diffraction data collected in oscillation mode. *Methods Enzymol.* **276**, 307–326 (1997).
35. Battye, T.G., Kontogiannis, L., Johnson, O., Powell, H.R. & Leslie, A.G. iMOSFLM: a new graphical interface for diffraction-image processing with MOSFLM. *Acta Crystallogr. D Biol. Crystallogr.* **67**, 271–281 (2011).
36. Vagin, A. & Teplyakov, A. Molecular replacement with MOLREP. *Acta Crystallogr. D Biol. Crystallogr.* **66**, 22–25 (2010).
37. Emsley, P. & Cowtan, K. Coot: model-building tools for molecular graphics. *Acta Crystallogr. D Biol. Crystallogr.* **60**, 2126–2132 (2004).
38. Murshudov, G.N., Vagin, A.A. & Dodson, E.J. Refinement of macromolecular structures by the maximum-likelihood method. *Acta Crystallogr. D Biol. Crystallogr.* **53**, 240–255 (1997).
39. Adams, P.D. *et al.* PHENIX: building new software for automated crystallographic structure determination. *Acta Crystallogr. D Biol. Crystallogr.* **58**, 1948–1954 (2002).
40. Laskowski, R.A., MacArthur, M.W., Moss, D.S. & Thornton, J.M. PROCHECK: a program to check the stereochemical quality of protein structures. *J. Appl. Crystallogr.* **26**, 283–291 (1993).
41. Taoka, M. *et al.* An analytical platform for mass spectrometry-based identification and chemical analysis of RNA in ribonucleoprotein complexes. *Nucleic Acids Res.* **37**, e140 (2009).

doi:10.1038/nsmb.2943